Biosensors and Bioelectronics 194 (2021) 113593

Contents lists available at ScienceDirect

Biosensors and Bioelectronics

journal homepage: www.elsevier.com/locate/bios

Development of antibody against drug-resistant respiratory syncytial virus: Rapid detection of mutant virus using split superfolder green fluorescent protein-antibody system

Hyeran Kim [a], Seul Gee Hwang [a], Kyeonghye Guk [a], Yoonji Bae [a], Hwangseo Park [b], Eun-Kyung Lim [a,c,**], Taejoon Kang [a,*], Juyeon Jung [a,***]

[a] Bionanotechnology Research Center, Korea Research Institute of Bioscience and Biotechnology (KRIBB), Daejeon, 34141, Republic of Korea
[b] Department of Bioscience and Biotechnology, Sejong University, Seoul, 05006, Republic of Korea
[c] Department of Nanobiotechnology, KRIBB School of Biotechnology, University of Science and Technology (UST), Daejeon, 34113, Republic of Korea

ARTICLE INFO

Keywords:
Antibody
Drug-resistance
S275F mutation
Respiratory syncytial virus
Green fluorescent protein

ABSTRACT

Respiratory syncytial virus (RSV) infections are associated with severe bronchiolitis or pneumonia. Although palivizumab is used to prevent RSV infections, the occurrence of palivizumab-resistant RSV strains is increasing, and these strains pose a threat to public health. Herein, we report an antibody with affinity to the S275F RSV antigen, enabling the specific detection of palivizumab-resistant RSV strains. Experimental and simulation results confirmed the affinity of the antibody to the S275F RSV antigen. Furthermore, we developed a rapid S275F RSV antigen detection method using a split superfolder green fluorescent protein (ssGFP) that can interact with the antibody. In the presence of the mutant virus antigen, ssGFP emitted fluorescence within 1 min, allowing the rapid identification of S275F RSV. We anticipate that the developed antibody would be useful for the precise diagnosis of antiviral drug-resistant RSV strains and help treat patients with RSV infections.

1. Introduction

Respiratory syncytial virus (RSV) is a single-stranded negative-sense RNA virus belonging to the genus *Orthopneumovirus* (Griffiths et al., 2017). Most individuals who contract an RSV infection exhibit mild illness and recover; however, infants, children, and elderly individuals are more likely to experience serious complications upon infection with RSV (ESimoes et al., 1999; Zhang et al., 2002). For example, RSV infections in children can cause bronchiolitis or pneumonia in 25–30% of cases, and in elderly individuals aged 65 years or above, it causes pneumonia which increases the mortality rate for these individuals (Simoes et al., 1999; Zhang et al., 2002). Moreover, 1–2% of all infected patients develop severe bronchiolitis requiring respiratory therapy or intensive care management (Simoes et al., 1999; Zhang et al., 2002). As the symptoms of RSV infection (congestion, runny nose, fever, cough, and sore throat) are similar to those of mild cold, accurate and rapid diagnosis is important for the timely treatment and medication of patients.

An RSV monoclonal antibody (palivizumab) and RSV immune globulin intravenous (RSV-IGIV) are commonly used for preventing and treating RSV infection (Collins et al., 2002). RSV-IGIV is produced using samples from donors with high levels of RSV-neutralizing antibodies, whereas palivizumab is produced using recombinant DNA technology (Collins et al., 2002). In recent days, the use of palivizumab has become more common as it can be administered via intramuscular injection and has fewer side effects than RSV-IGIV (Collins et al., 2002). Although palivizumab has been successfully used for suppressing severe RSV infection in high-risk individuals, its overuse has induced the development of palivizumab resistance in RSV strains (Adams et al., 2010).

Reportedly, the RSV genome encodes for 11 proteins, of which the fusion protein (F protein) that mediates the fusion between the virus and the host membranes is responsible for infection (Adams et al., 2010; Zhu et al., 2012). Palivizumab neutralizes the RSV by binding to the F protein; therefore, mutations in the F protein of the RSV are associated with palivizumab resistance (Adams et al., 2010; Zhu et al., 2012). Previous studies have shown that the half-maximal inhibitory concentration

* Corresponding author. Bionanotechnology Research Center, KRIBB, Daejeon, 34141, Republic of Korea.
** Corresponding author. Bionanotechnology Research Center, KRIBB, Daejeon, 34141, Republic of Korea.
*** Corresponding author. Bionanotechnology Research Center, KRIBB, Daejeon, 34141, Republic of Korea.
E-mail addresses: eklim1112@kribb.re.kr (E.-K. Lim), kangtaejoon@kribb.re.kr (T. Kang), jjung@kribb.re.kr (J. Jung).

https://doi.org/10.1016/j.bios.2021.113593
Received 23 February 2021; Received in revised form 30 June 2021; Accepted 24 August 2021
Available online 26 August 2021

(IC50) of palivizumab for wild-type (WT) RSV is 0.49 μg/mL, whereas it is > 100 μg/mL for S275F RSV, which is a representative palivizumab-resistant RSV mutant strain (Zhu et al., 2012). Considering that the emergence of palivizumab-resistant strains could pose an unprecedented threat to public health, it is critical to accurately and rapidly diagnose palivizumab-resistant RSV infections so that RSV-infected patients can receive proper treatment.

For RSV detection, several types of antigen-sensing and polymerase chain reaction (PCR)-based methods have been developed (Son et al., 2015; Mahony et al., 2011; Brendish et al., 2015; Popow-Kraupp et al., 2011). Some of the methods approved by the U.S. Food and Drug Administration (FDA) are used for the diagnosis of RSV infection. However, Rapid antigen assays for the identification of mutant RSV strains are yet to be developed, and this includes the development of the antibody against drug-resistant RSV. The conventional PCR is designed to detect RSV, simply indicating the presence of RSV in the sample. To determine whether the RSV contained in the sample is resistant to palivizumab, the analysis through sequencing is required. Although previous studies suggested the PCR-based identification of palivizumab-resistant RSV (Griffiths et al., 2017), the PCR-based detection methods require the extraction of nucleic acids by rupturing the virus, which might affect the yield of viral nucleic acids and the subsequent results. Therefore, the detection of palivizumab-resistant RSV by current methods is not suitable enough for situations where appropriate treatment is required immediately. This prompted us to develop a rapid detection approach for palivizumab-resistant RSV including a secure of a novel antibody.

In this study, we aim to develop a rapid detection approach for palivizumab-resistant RSV using a novel antibody. Further, we demonstrate the potential of the developed ssGFP-antibody system to detect the S275F virus in real human samples. This is the first study to report an antibody against the S275F RSV antigen. The antibody was developed using a phage display library, and the antibody showed a binding affinity (K_d) of 2.70 nM for the S275F RSV antigen. The homology modeling results of the antibody and S275F RSV also confirmed the experimental affinity. Furthermore, we developed a split superfolder green fluorescent protein (ssGFP)-antibody system for rapid and accurate detection of the S275F RSV antigen. When the S275F RSV antigen was present with the ssGFP-antibody system, ssGFP emitted fluorescence. This system allowed the detection of the S275F RSV antigen at a concentration as low as 1.8 pM. More importantly, the ssGFP-antibody system can detect the mutant RSV antigen within 1 min. It is anticipated that the developed antibody and the rapid mutant RSV antigen assay will be useful for the precise diagnosis of antiviral drug-resistant RSV and selection of the appropriate therapeutic regimen for the patients.

2. Materials and methods

2.1. Production of proteins

The codon-optimized RSV F gene (GenBank: FJ614814) was synthesized by Bioneer (Korea), amplified by PCR with primers (Table S1), and cloned into a pcDNA3.1/myc-His(−)A vector via digestion at the *Nhe*I and *Xho*I sites. The S275F RSV mutation was introduced using PCR with primers (Table S2). The prepared plasmids were transfected into Expi293F™ Cells (Thermo Fisher Scientific Inc., MA, USA) using the ExpiFectamine™ 293 Transfection Kit (Life Technologies, NY, USA) according to the manufacturer's instructions. The cells were incubated in the Expi293™ Expression Medium (Life Technologies) for 3 days at 37 °C at 8% CO_2. After incubation, the cells were harvested, suspended in lysis buffer (50 mM Tris-HCl, 5 mM 2-mercaptoethanol, 100 mM KCl, and 1 mM phenylmethylsulfonyl fluoride, pH 8.5, Sigma-Aldrich, MO, USA), sonicated, and centrifuged at 16,000×*g* for 15 min at 4 °C. The soluble proteins from the cell supernatant were applied to IDA Excellose (Bioprogen, Korea) and eluted with an elution buffer (50 mM Tris-HCl, 0.5 M NaCl, and 0.5 M imidazole, pH 8.0, Sigma-Aldrich). The purified proteins were dialyzed with phosphate-buffered saline (PBS, Sigma-Aldrich) and purified using Q-Sepharose anion-exchange chromatography (GE Healthcare, IL, USA). Bovine serum albumin (BSA) was purchased from Sigma-Aldrich.

2.2. Production of VLPs

Virus-Like particles (VLPs) consisting of an influenza virus matrix (M1) protein and WT RSV or S275F RSV F proteins were generated. The reverse genetics system used to generate VLPs was kindly gifted by Dr. Meehyein Kim of Korea Research Institute of Chemical Technology (KRICT). M1 genes derived from A/Puerto Rico/8/1934 (H1N1) genomic RNA were cloned individually into pVP-M vector using universal reverse primers and genome-specific primers. In addition, WT and S275F RSV F proteins were introduced within the F fragment by the forward primer: 5′-TATTCGTCTCAGGGAGCAAAAGCAGGACTTTAAAATGGAGCTGCTGATCCTG-3′ and reverse primer: 5′-ATATCGTCTCGTATTAGTAGAAACAAGGAGTTTTTTGAACAGATCAGTGGTGGTGGTGGTGGTG-3'. In detail, co-cultured 293T and Madin-Darby Canine Kidney (MDCK) cells (0.5×10^6 cells per well) were transfected with WT or S275F RSV and M1 plasmids. At 3–6 days post-transfection, cell supernatants were titrated to HEp-2 cell monolayers to estimate virus titers. VLPs were concentrated with QuixStand (GE Healthcare) and purified via a discontinuous sucrose gradient at 14,000×*g* for 1 h at 4 °C. The VLP bands between 30 and 60% were collected and centrifuged at 14,000×*g* for 40 min at 4 °C. VLPs were characterized by Western blots using 6 × -His Tag monoclonal antibody (MA1-21315, Invitrogen, MA, USA) to probe RSV F protein and anti-M1 antibody to detect M1 protein (Fig. S1).

2.3. Production of antibody against S275F RSV antigen

The antibody specific to the S275F RSV antigen was selected from the synthetic fragment antigen-binding (Fab) phage display library. For bio-panning, a round tube (5 mL) was coated with 100 μg of the antigen (WT and S275F) in 1 mL of carbonate-bicarbonate buffer (Sigma-Aldrich) for 12 h at 4 °C and blocked by treating with 5% skim milk (Sigma-Aldrich) in PBS for 1 h at 37 °C.

The Fab phage library stock was used to inoculate 100 mL of yeast extract tryptone (YT, 2 ×) broth (Sigma-Aldrich) supplemented with ampicillin (100 μg/mL, Sigma-Aldrich) and incubated in a shaking incubator at 37 °C until the optical density at 600 nm (OD_{600}) reached 0.6. Next, a helper phage (10^{12} plaque-forming unit (PFU)/mL) was used to inoculate the medium and incubated for 1 h at 37 °C. Next, kanamycin (70 μg/mL, Sigma-Aldrich) was added and incubated for 12 h at 37 °C. The prepared library was centrifuged at 10,000×*g* for 20 min. The supernatant (100 mL) was mixed with 4 g of polyethylene glycol (Sigma-Aldrich) and 3 g of NaCl and incubated in ice for 1 h. Afterward, the mixture was centrifuged at 16,000×*g* for 30 min, and the pellet was resuspended in 1 mL of PBS. The resuspended phage was centrifuged again at 16,000×*g* for 10 min, and 900 μL of the supernatant was transferred to the WT RSV antigen-coated tube and incubated for 1 h at 37 °C.

The Fab phage in the WT RSV antigen-coated tube was transferred to the S275F RSV antigen-coated tube and incubated for 2 h at 37 °C. The S275F-coated tube was washed several times with PBS with 0.05% Tween-20 (PBST, Sigma-Aldrich), and the residual phage was eluted with 1 mL of Tris glycine-HCl (0.1 M, pH 2.5). Next, the elute was neutralized with 80 μL of Tris-HCl (1 M, pH 9.0, Sigma-Aldrich). The eluted phage was used to infect 10 mL of TG1 cell culture ($OD_{600} = 0.6$) in 2 × YT broth at 37 °C and incubated for 1 h at 37 °C. The infected cells were centrifuged at 10,000×*g* for 5 min, and the pellet was resuspended in 1 mL of 2 × YT media. The resuspended cells were seeded in a plate with 2 × YT agar supplemented with ampicillin and incubated for 12 h at 37 °C. Post the amplification step, the phage was subjected to another

round of panning, as described above, and the final four rounds of panning were performed. TG1 cells were incubated with final round output Fab-phages, and infected colonies were randomly screened to select S275F specific Fab clones by measuring the absorbance at 450 nm using a microplate reader (Perkin Elmer, MA, USA).

To convert the selected Fab to whole immunoglobulin G (IgG), the CH and VK sequences of the selected colony were amplified by PCR with the corresponding primers (Tables S3 and S4). The amplified DNA and pdCMV-dhfrC vector were digested using A*pa*I/*Eco*RI-HF for the heavy chain region and *Hin*dIII/*Bsi*WI for the light chain region. Next, the DNA was ligated with the ligation mixture for 1 h at 16 °C, and the resultant ligates were used to transform DH5-alpha cells, which were then cultured for 12 h at 37 °C. After culturing, DNA was purified from the colony using a DNA Prep Kit (Biofact, Daejeon, Korea) and transfected into Expi293F™ Cells using the ExpiFectamine™ 293 Transfection Kit according to the manufacturer's protocol. The cells were incubated in the Expi293™ Expression Medium for 3 days at 37 °C under 8% CO_2. After incubation, whole antibodies were purified using a protein A resin (Millipore, MA, USA). Briefly, the resin-bound antibodies were washed with Dulbecco's PBS (DPBS) and eluted with 10 mL of Tris glycine-HCl (0.1 M, pH 2.5). The eluted antibody was neutralized with 800 μL of Tris-HCl (1 M, pH 9.0) and buffer-exchanged with DPBS.

2.4. ELISA

For phage-based enzyme-linked immunosorbent assay (ELISA), 100 ng of the proteins (S275F, WT, BSA, and PBS) were coated on a 96-well plate (Thermo Fisher Scientific Inc.), incubated for 12 h at 4 °C, and blocked by treating with 2% skim milk in PBS for 1 h at 37 °C. Next, the purified phage was added to the well plate and incubated for 2 h at 37 °C. The 96-well plate was washed with PBST, following which anti-M13 antibody-horseradish peroxidase (HRP) (Thermo Fisher Scientific Inc.) was added (1:2000 dilution in PBS). After incubation for 1 h at 37 °C, the plate was washed with PBST, followed by the addition of 100 μL of tetramethylbenzidine (TMB, Thermo Fisher Scientific Inc.) and 50 μL of H_2SO_4 (1 M, Sigma-Aldrich). Absorbance was measured at 450 nm using Multiscan FC (Thermo Fisher Scientific Inc.). Fab-based ELISA was performed using the same method using purified Fab instead of the phage.

To measure the binding affinities of the antibody to the S275F and WT antigens, 100 ng of the antigens were coated in a 96-well plate and incubated for 12 h at 4 °C, and were blocked by treating with 2% skim milk in PBS for 1 h at 37 °C. Next, the antibody (0–50 nM) was added to the well plate and incubated for 2 h at 37 °C. The commercially available anti-RSV F protein antibody (Ab94968, Abcam, UK) was also used to confirm the antigenicity of the antigens. The plate was washed with PBST, and anti-human IgG FC-HRP (Thermo Fisher Scientific Inc.) was added (1:2000 dilution in DPBS). After incubation for 1 h at 37 °C, the plate was washed with PBST, followed by the addition of 100 μL of TMB solution and 50 μL of H_2SO_4 (1 M). The absorbance was measured at 450 nm using Multiscan FC.

To measure the binding affinity of the antibody against ssGFP, 100 ng of ssGFP was coated in a 96-well plate and incubated for 12 h at 4 °C, and blocked by treating with 2% skim milk in PBS for 1 h at 37 °C. Next, the antibody (0–250 nM) was added to the well plate and incubated for 2 h at 37 °C. The plate was washed with PBST, and anti-human IgG FC-HRP was added (1:2000 dilution in DPBS). After incubation for 1 h at 37 °C, the plate was washed with PBST, followed by the addition of 100 μL of TMB solution and 50 μL of H_2SO_4 (1 M). The absorbance was measured at 450 nm using Multiscan FC.

2.5. Dot-blot test

VLPs (WT and S275F) were blotted onto nitrocellulose membrane and air-dried. Next, the membrane was incubated with palivizumab or developed antibody (1 μ/mL) in BSA/PBST for 2 h at 37 °C. Bound antibody was detected using a goat Anti-Human IgG-HRP antibody (1:3,000, Thermo Fisher Scientific Inc.) and enhanced chemiluminescent reagent (Thermo Fisher Scientific Inc.) using a chemiDOC M.D. gel documentation system (Bio-rad, CA, USA).

2.6. Homology modeling of antibody and docking simulations with model epitope

Because the three-dimensional (3D) structure of the antibody is yet to be determined, homology modeling was performed using the X-ray crystal structure of the vascular endothelial growth factor-binding variant of the G6 Fab antibody as the structural template (PDB entry: 3AUV). The sequence identity between the antibody and the template was 84% (Fig. S2), which allowed us to obtain the atomic coordinates of the antibody successfully using homology modeling. The ClustalW program was used to align the amino acid sequences of the antibody and the structural template according to BLOSUM matrices for scoring the alignments. The best-scored sequence alignment served as the input for constructing the 3D structural model for the antibody using the MODELLER program version 8v2. The structural models for the epitopes were prepared based on the X-ray crystal structure of the RSV F protein (PDB entry: 5C6B). These simplified epitope models comprised eleven amino acids in the sequence of QKKLMSNNVQI for WT and QKKLMFNNVQI for the S275F mutant.

To determine the binding affinities and binding modes of the WT and S275F mutant epitopes with respect to the antibody, docking simulations were performed in complementarity-determining regions (CDRs) of the antibody using the AutoDock program. The modified binding free energy function involving an accurate hydration term was adopted based on its high performance in estimating protein-ligand interactions. Docking simulation of an epitope commenced with the calculation of 3D grids of interaction energy in the CDR for all atom types present in the model epitopes. The calculated grid maps had the dimension of 61 × 61 × 61 points with a spacing of 0.375 Å, producing a receptor model in which the antibody atoms were included within 22.9 Å of the grid center. For both WT and S275F mutant epitopes, 20 docking runs were performed with the initial population of 50 individuals. Among the 20 conformations of a model epitope generated during the docking simulations, those clustered together showed similar binding conformations differing by less than 1.5 Å in positional root-mean-square deviation values.

2.7. Split superfolder green fluorescent protein (ssGFP) production

Superfolder GFP sequence generated by *in vitro* manipulation of the GFP gene derived from Aequorea Victoria was selected (Pe'delacq et al., 2006). The ssGFP consisted of ligation of three fragments, including the 1st–10th β-strands of GFP, a linker, and the 11th β-strand of GFP. The 1st–10th β-strands and 11th β-strand sequences of GFP were amplified by PCR using primers shown in Table S5. The amplified DNA fragment containing 1st–10th β-strand nucleotide sequence of the GFP was digested with *Nde*I/*Spe*I, cloned into a pET21a vector, digested with *Bam*HI/*Eco*RI, and then cloning of the 11th β-strand was performed. The scheme of vector construction is summarized in Fig. S3. The cloned plasmid was digested using *Spe*I/*Bam*HI and ligated with a linker amplified by PCR with appropriate primers (Table S5). The agarose gel electrophoresis images of the PCR results for the ssGFP construction are shown in Fig. S4. The prepared plasmid was used to transfect *Escherichia coli* BL21 (DE3) cells and cultured in 0.2 L of 2 × YT broth supplemented with ampicillin (100 μg/mL) at 37 °C until the OD_{600} value reached 0.6. The BL21 (DE3) culture was further induced with 1 mM (final concentration) isopropyl β-D-1-thiogalactopyranoside (Sigma-Aldrich) and incubated for 4 h at 37 °C. The cells were harvested, washed with Tris-HCl (50 mM) and ethylenediaminetetraacetic acid (1 mM, pH 8.0, Sigma-Aldrich), centrifuged at 10,000×*g* for 10 min, and resuspended in buffer (50 mM Tris-HCl and 0.2 M NaCl). The resuspended cells were

sonicated and centrifuged at 16,000×*g* for 30 min. The soluble proteins from the cell supernatant were purified using a Fast Protein Liquid Chromatography System (Bio-rad) with Ni-NTA (Qiagen, Germany) resin at a flow rate of 4 mL/min. The resin-bound proteins were washed with buffer (50 mM Tris-HCl, 0.2 M NaCl, and 10% glycerol, pH 7.4) and eluted with an elution buffer (50 mM Tris-HCl, 0.2 M NaCl, 10% glycerol, and 0.5 M imidazole, pH 7.4). The elute was dialyzed with PBS and concentrated to 1 mg/mL (final concentration).

2.8. Detection of S275F RSV antigen using ssGFP-antibody system

To prepare the Cy5-conjugated antibody, 90 μL of the antibody (50 nM) was mixed with 150 μL of Cy5 N-hydroxysuccinimide (NHS) ester (0.48 mg in dimethyl sulfoxide, Abcam) and maintained for 45 min at 25 °C. After the reaction, the buffer was exchanged with DPBS. For immobilization of the ssGFP-antibody on a glass slide, 3 μL of ssGFP (2.5 μM) was coated on an aldehyde glass slide (Arrayit Corporation, CA, USA) via reaction with N-ethyl-N'-(3-(dimethylamino) propyl) carbodiimide (0.1 M, Sigma-Aldrich) and NHS (0.4 M, Sigma-Aldrich) for 5 min. After washing the glass with DPBS, 3 μL of Cy5-conjugated antibody (50 nM) was coated on the slide and washed with DPBS after 1 h. To detect RSV antigens, 3 μL of protein (5 μM, WT and S275F) was reacted on the ssGFP-antibody-coated glass for 15 min and washed with DPBS. Fluorescence signals were detected using Axon GenePix 4200A (Molecular Devices, CA, USA) with an Alexa-488 filter for green fluorescence and a Cy5 filter for red fluorescence.

To construct the ssGFP-antibody system, ssGFP (50 nM) and BSA (40 nM) were mixed and incubated for 1 h at 25 °C. Next, the antibody (50 nM) was added and incubated for 10 min at 25 °C. To detect the S275F RSV antigen, 200 μL of protein was added to the ssGFP-antibody system (200 μL). The fluorescence signal was measured using a microplate reader (BioTek, VT, USA) at an excitation wavelength of 475 nm and an emission wavelength of 510 nm. For the detection of VLPs (WT and S275F), 200 μL of the prepared VLPs (10^3 PFU/mL) or 200 μL of VLP-spiked nasopharyngeal swab samples (10^3 PFU/mL) was added to the ssGFP-antibody system (200 μL), and the fluorescence signal was measured using a microplate reader at an excitation wavelength of 475 nm and an emission wavelength of 510 nm.

3. Results and discussion

The nucleotide and amino acid sequences of the antibody against the S275F RSV antigen are provided in Fig. 1a. The CDRs of the heavy and light chains are colored red. For the development of the antibody, the Fab phage was selected from a large human Fab phage display library through four rounds of bio-panning, including a subtraction for the WT RSV antigen. The WT and S275F RSV antigens were prepared using PCR, cloning, transfection, and expression procedures. The antigenicity of the prepared antigens confirmed by a commercially available anti-RSV F protein antibody (Fig. S5). The selected phage and the purified Fab exhibited high affinity to the S275F RSV antigen, as shown in Fig. 1b. In addition, the signals obtained in the ELISA increased significantly when the mutant antigen was present, whereas weak signals were observed for the WT antigen, BSA, and PBS. The selected Fab was converted to full-length IgG as the final monoclonal antibody, purified, and stored for further applications.

After antibody production, K_d of the antibody was determined as the S275F antigen concentration required to inhibit 50% of binding activity by ELISA. K_d value of the antibody was calculated to be 2.70 nM from the Klotz plot (Fig. S6). Furthermore, the developed antibody was strongly bound to the S275F RSV antigen in a concentration-dependent manner, while the antibody exhibited a low binding affinity to the WT RSV antigen (Fig. 1c). These results confirmed that the developed antibody could be employed for the identification of palivizumab-resistant RSV.

To investigate whether the binding affinity of the antibody to the S275F RSV antigen is higher than that to the WT antigen, we performed computational modeling for the associated antibody-epitope interaction analysis. As shown in Fig. 2, the binding free energies of the S275F (QKKLMFNNVQI) and WT (QKKLMSNNVQI) RSV epitopes to the CDRs of the antibody were calculated to be −15.8 and −12.0 kcal/mol, respectively. The S275F mutant epitope appeared to bind more extensively to the CDRs of the antibody than the WT epitope, which was consistent with the experimental results. The binding modes of the S275F and WT RSV epitopes in the CDRs of the antibody are further

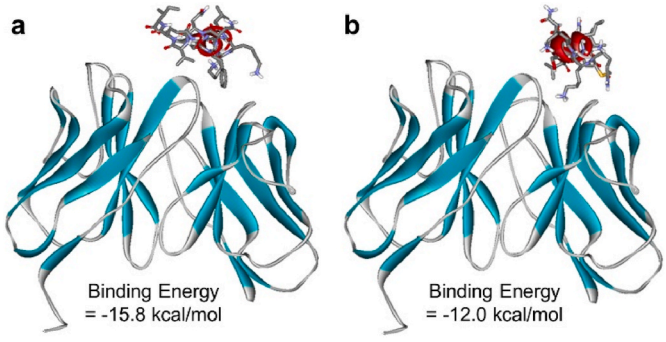

Fig. 2. Docked poses of epitopes of (**a**) S275F and (**b**) WT RSV in CDRs of antibody.

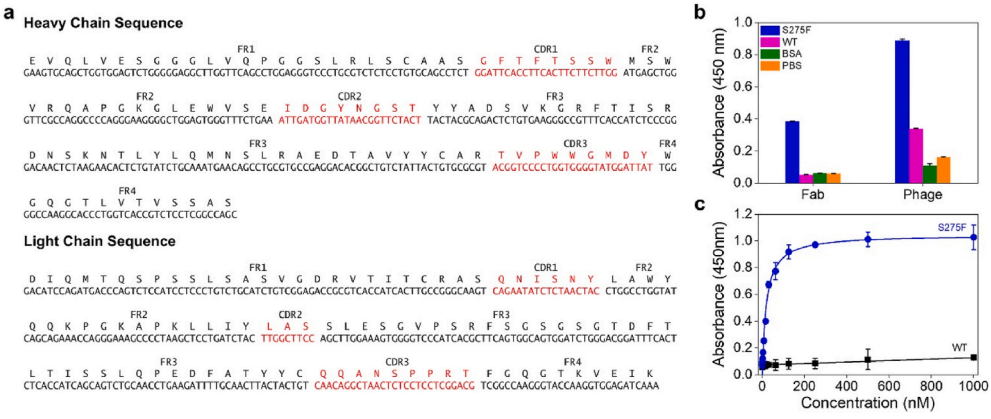

Fig. 1. (**a**) Nucleotide and amino acid sequences of antibody against S275F RSV antigen. (**b**) Results of Fab- and phage-based ELISA using S275F and WT RSV antigens, BSA, and PBS. Data is represented as mean +standard deviation of three measurements. (**c**) Results of ELISA using antigens (S275F and WT) at increasing concentrations of antibody. Data is represented as mean ± standard deviation of three measurements.

compared in Fig. S7. This simulation results confirmed that the substitution of Phe for Ser at residue 275 of the RSV F protein increased the antibody binding affinity.

For the simple and rapid identification of the S275F RSV antigen, we designed the ssGFP, which could bind to the antibody (Fig. 3a). The green fluorescent protein (GFP) is considered an excellent tool in multiple domains of biological research, such as biosensing, bioimaging, gene delivery, and transfection (Pe'delacq et al., 2006; Romej et al., 2019; Feng et al., 2017; Lindman et al., 2010; Jiang et al., 2016). In particular, the molecular engineering of GFP has enabled the formation of split GFP, which is widely used in the field of biosensing (Pe'delacq et al., 2006; Romej et al., 2019; Feng et al., 2017; Lindman et al., 2010; Jiang et al., 2016). GFP-based sensing techniques are simple, easy to implement, and emit fluorescence signals that can be measured via routine processes (Pe'delacq et al., 2006; Romej et al., 2019; Feng et al., 2017; Lindman et al., 2010; Jiang et al., 2016). We constructed ssGFP containing three fragments: the 1st–10th β-strands of GFP, a linker, and the 11th β-strand of GFP. The semiflexible linker enabled the two fragments of ssGFP to be positioned proximally or distally. When the two fragments of ssGFP were separated, no fluorescence signals were emitted. When the distance between the divided N-terminal partial fragment and the C-terminal fragment of ssGFP was reduced, green fluorescence signals were generated. In addition, the linker contained epitopes (NSELLSLIDDMPITNDQKKLMSNN) for interaction with the antibody, allowing the formation of the ssGFP-antibody complex. Fig. 3b shows the results of ELISA using ssGFP and the antibody. The absorbance value increased with the increase in the antibody concentration. Furthermore, the K_d value of the antibody to the ssGFP was estimated to be 42.78 nM by ELISA. These results indicated the feasibility of the formation of the ssGFP-antibody complex. Next, we compared the fluorescence signals of bare ssGFP and ssGFP-antibody complexes (Fig. 3c). The bare ssGFP emitted distinct green fluorescence, whereas the ssGFP-antibody complex emitted considerably weak fluorescence signals, as antibody binding induced the separation of the ssGFP fragments. Of note, the fluorescence signals of ssGFP were quenched almost immediately after it bound to the antibody. Moreover, the binding affinity of the antibody to ssGFP (42.78 nM) was approximately 15 times weaker than that of the antibody to the S275F RSV antigen (2.70 nM). From these findings, we inferred that this unique property of ssGFP could allow the rapid and accurate detection of the mutant RSV antigen.

To examine whether the ssGFP-antibody system could distinguish between the WT and S275F RSV antigens, we prepared the ssGFP-antibody-Cy5 system chip and assessed the identification of antigens using the chip (Fig. S8). It was observed that when the S275F RSV antigen was reacted with the ssGFP-antibody-Cy5 chip, the mutant antigen was first bound to the Cy5-conjugated antibody and then released from the chip, and the residual ssGFP emitted green fluorescence. In contrast, the ssGFP-antibody-Cy5 complex was preserved on the glass after the reaction with the WT RSV antigen, in which red fluorescence signals were emitted by Cy5. This shows that the ssGFP-antibody system could successfully identify the S275F RSV antigen.

Next, we assessed the rapid identification of the S275F RSV antigen using the ssGFP-antibody system. As shown in Fig. 4a, the prepared ssGFP-antibody complex barely emitted fluorescence signals in a tube. However, upon the addition of the mutant RSV antigen, green fluorescence emission by ssGFP commenced rapidly (within 1 min). When the WT RSV antigen was added, no change was observed in the fluorescence signal. Fig. S9 shows the green fluorescence signals obtained 1 min after adding the S275F and WT RSV antigens (100 nM). Strong fluorescence signals were detected only after the S275F RSV antigen was added. Additionally, we attempted to detect the mutant RSV antigen (Fig. 4b) quantitatively. As the target antigen concentration increased, the fluorescence intensity also increased. Based on the limit of detection (LOD) = 3 sd/m, where sd represents the standard deviation of fluorescence signals for control samples and m represents the slope of the linear calibration curve, the LOD was estimated to be 1.8 pM (inset of Fig. 4b).

Finally, we demonstrate whether the developed ssGFP-antibody

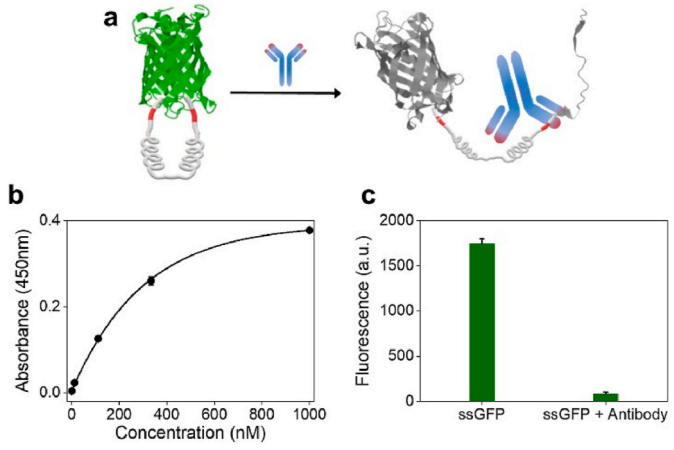

Fig. 3. (**a**) Schematic illustration of ssGFP-antibody system. Bare ssGFP emitted strong green fluorescence signals, whereas ssGFP-antibody complex emitted weak signals. (**b**) Results of ELISA using ssGFP at increasing antibody concentrations. Data is represented as mean ± standard deviation of three measurements. (**c**) Fluorescence signals of bare ssGFP and ssGFP-antibody complex. Data is represented as mean +standard deviation of three measurements.

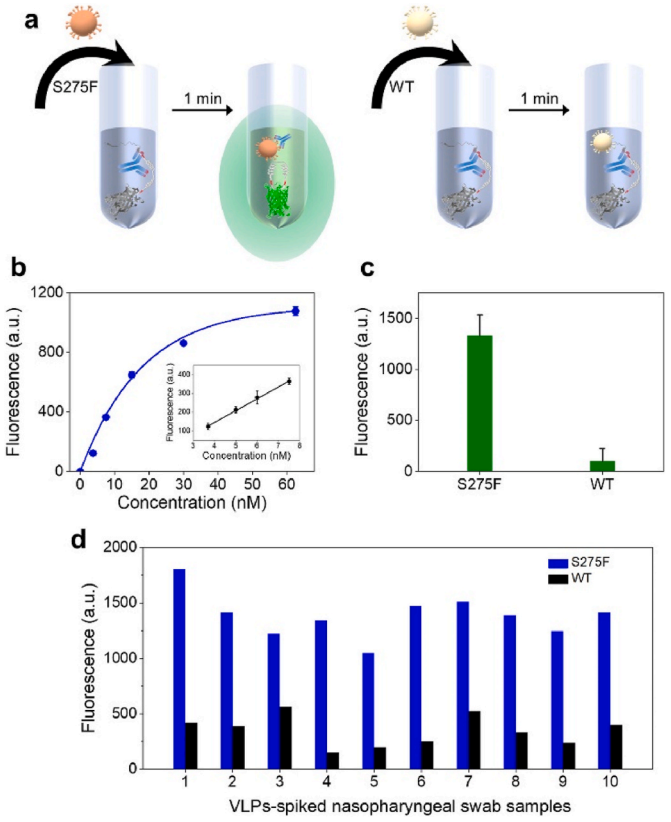

Fig. 4. (**a**) Schematic illustration of S275F RSV detection using ssGFP-antibody system. Green fluorescence signals are detected within 1 min in the presence of S275F RSV. (**b**) Plot of fluorescence signal *versus* concentration of S275F RSV antigen. Inset is magnified plot of fluorescence signal *versus* concentration of S275F RSV antigen. Data is represented as mean ± standard deviation of 10 measurements. (**c**) Fluorescence signals after detection of S275F and WT RSV VLPs using ssGFP-antibody system. Data is represented as mean +standard deviation of three measurements. (**d**) Fluorescence signals after detection of S275F (blue bars) and WT (black bars) VLPs in human nasopharyngeal swab samples.

system can detect the S275F virus in real human samples. Since the current diagnosis in the hospital does not confirm the presence of antiviral drug resistance of RSV, we prepared the VLPs consisting of an influenza virus M1 protein and WT RSV or S275F RSV F proteins. As shown in Fig. S10, the WT and S275F VLPs were well-structured and properly assembled. Fig. 1c represents the green fluorescence signals after adding the S275F and WT RSV VLPs (10^3 PFU/mL) into the ssGFP-antibody systems, respectively. Strong fluorescence signals were obtained only after the S275F VLP was added. Furthermore, we spiked the VLPs into the nasopharyngeal swab samples collected from symptomatic patients. The bare nasopharyngeal swab samples were negatively diagnosed for RSV. As shown in Fig. 4d, strong green fluorescence emission was observed in the presence of S275F mutant VLPs, whereas the fluorescence signal was much lower in the presence of WT RSV VLPs in nasopharyngeal swab samples. Based on these results, we inferred that the developed ssGFP-antibody system could specifically detect the S275F RSV in real samples. Of note, the developed approach is the first rapid palivizumab-resistant RSV antigen detection method with the potential for the accurate on-site identification of mutant RSV.

4. Conclusions

Infectious viruses pose a major threat to human beings (Wang et al., 2020). The ongoing pandemic caused by the severe acute respiratory syndrome coronavirus 2 has severely affected humankind in the past year (Wang et al., 2020). Since the outbreak cycle of the emerging virus has shortened over time, it is necessary to investigate and respond to various infectious diseases (Luo et al., 2020). To date, several types of viral infections have affected humans globally; however, the threats have been mitigated effectively by developing effective antiviral drugs and vaccines (Afrough et al., 2019). Unfortunately, the possibility of virus re-emergence has increased as viruses have developed resistance to various drugs (Eom et al., 2019a; Eom et al., 2019b; Kim et al., 2021; Moon et al., 2020; Guk et al., 2020; Hwang et al., 2018). Moreover, because it is difficult to treat or prepare vaccines against mutant viruses, it is critical to diagnose such viral infections rapidly and accurately to prevent their spread (Eom et al., 2019a; Eom et al., 2019b; Kim et al., 2021; Moon et al., 2020; Guk et al., 2020; Hwang et al., 2018). We have previously attempted to develop immunological assays for the rapid diagnosis of drug-resistant influenza viruses (Eom et al., 2019a; Eom et al., 2019b; Kim et al., 2021; Moon et al., 2020; Guk et al., 2020; Hwang et al., 2018). In this study, we widened the diagnostic target to RSV and successfully developed the antibody against the S275F RSV antigen for the first time. The antibody exhibited a K_d value of 2.70 nM toward the mutant RSV antigen, and the modeling results supported the affinity. Furthermore, we constructed the ssGFP system by adding the mimotope of the S275F RSV antigen, which successfully and efficiently formed the ssGFP-antibody complex. The findings demonstrate that the ssGFP-antibody system reacts rapidly in the presence of the S275F RSV antigen, enabling the detection of the mutant RSV antigen within 1 min. This rapidity makes the current approach suitable for the on-site diagnosis of mutant RSV, even in resource-poor settings. We expect that the antibody and the rapid S275F RSV antigen sensing system developed in the present study would be useful for diagnosing and treating RSV-infected patients.

Data availability

The datasets used and/or analyzed during the current study are available from the corresponding author upon reasonable request.

CRediT authorship contribution statement

Hyeran Kim: Methodology, Validation, Formal analysis, Investigation, Data curation, Writing – review & editing. **Seul Gee Hwang:** Methodology, Validation, Formal analysis, Investigation, Data curation, Writing – original draft. **Kyeonghye Guk:** Validation, Investigation, Data curation. **Yoonji Bae:** Validation, Investigation. **Hwangseo Park:** Software, Resources, Writing – original draft, Visualization. **Eun-Kyung Lim:** Conceptualization, Funding acquisition. **Taejoon Kang:** Data curation, Writing – original draft, Writing – review & editing, Visualization, Supervision, Project administration, Funding acquisition. **Juyeon Jung:** Conceptualization, Methodology, Validation, Resources, Writing – original draft, Writing – review & editing, Supervision, Project administration, Funding acquisition.

Declaration of competing interest

The authors declare that they have no known competing financial interests or personal relationships that could have appeared to influence the work reported in this paper.

Acknowledgments

This research was supported by National R&D Programs through National Research Foundation (NRF) of Korea funded by Ministry of Science and ICT (MSIT) of Korea (NRF-2020R1A2C1010453, NRF-2021M3E5E3080844, NRF-2019R1C1C1006867, NRF-2021M3H4A1A02051048, NRF-2021M3E5E3080379, and NRF-2018M3A9E2022821), Global Frontier Program through Center for BioNano Health-Guard funded by MSIT of Korea (H-GUARD_2014M3A6B2060507 and H-GUARD_2013M3A6B2078950), Technology Development Program for Biological Hazards Management in Indoor Air through Korea Environment Industry & Technology Institute (KEITI) funded by Ministry of Environment (ME) of Korea (2021003370003), Industrial Technology Alchemist Program funded by Ministry of Trade, Industry, and Energy (MOTIE) of Korea (20012435), Nanomedical Devices Development Program of National Nano Fab Center (CSM2105M101), and KRIBB Research Initiative Program (1711134081 and 1711134038).

Appendix A. Supplementary data

Supplementary data to this article can be found online at https://doi.org/10.1016/j.bios.2021.113593.

References

Adams, O., Bonzel, L., Kovacevic, A., Mayatepek, E., Hoehn, T., Vogel, M., 2010. Clin. Infect. Dis. 51, 185–188, 2010.
Afrough, B., Dowall, S., Hewson, R., 2019. Clin. Exp. Immunol. 196, 157–166, 2019.
Brendish, N.J., Schiff, H.F., Clark, T.W., 2015. J. Infect. 71, 501–510, 2015.
Collins, P.L., Murphy, B.R., 2002. Virology 296, 204–211, 2002.
Eom, G., Hwang, A., Kim, H., Yang, S., Lee, D.K., Song, S., Ha, K., Jeong, J., Jung, J., Lim, E.-K., Kang, T., 2019a. ACS Sens. 4, 2282–2287, 2019.
Eom, G., Hwang, A., Lee, D.K., Guk, K., Moon, J., Jeong, J., Jung, J., Kim, B., Lim, E.-K., Kang, T., 2019b. ACS Appl. Bio. Mater. 2, 1233–1240, 2019.
Feng, S., Sekine, S., Pessino, V., Li, H., Leonetti, M.D., Huang, B., 2017. Nat. Commun. 8, 1–10, 2017.
Griffiths, C., Drews, S.J., Marchant, D.J., 2017. Clin. Microbiol. Rev. 30, 277–319, 2017.
Guk, K., Kim, H., Lee, M., Choi, Y.-A., Hwang, S.G., Han, G., Kim, H.-N., Kim, H., Park, H., Yong, D., Kang, T., Lim, E.-K., Jung, J., 2020. Nat. Commun. 11, 3418, 2020.
Hwang, S.G., Ha, K., Guk, K., Lee, D.K., Eom, G., Song, S., Kang, T., Park, H., Jung, J., Lim, E.-K., 2018. Sci. Rep. 8, 12999, 2018.
Jiang, W.-X., Dong, X., Jiang, J., Yang, Y.-H., Yang, J., Lu, Y.-B., Fang, S.-H., Wei, E.-Q., Tang, C., Zhang, W.-P., 2016. Sci. Rep. 6, 20568, 2016.
Kim, H., Kang, H., Kim, H.-N., Kim, H., Moon, J., Guk, K., Park, H., Yong, D., Bae, P.K., Park, H.G., Lim, E.-K., Kang, T., Jung, J., 2021. Biosens. Bioelectron. 187, 113324, 2021.
Lindman, S., Hernandez-Garcia, A., Szczepankiewicz, O., Frohm, B., Linse, S., 2010. Proc. Natl. Acad. Sci. U.S.A. 107, 19826–19831, 2010.
Luo, G., Gao, S.-J., 2020. J. Med. Virol. 92, 399–400, 2020.
Mahony, J.B., Petrich, A., Smieja, M., 2011. Crit. Rev. Clin. Lab Sci. 48, 217–249, 2011.
Moon, J., Kwon, H.-J., Yong, D., Lee, I.-C., Kim, H., Kang, H., Lim, E.-K., Lee, K.-S., Jung, J., Park, H.G., Kang, T., 2020. ACS Sens. 5, 4017–4026, 2020.
Pédelacq, J.-D., Cabantous, S., Tran, T., Terwilliger, T.C., Waldo, G.S., 2006. Nat. Biotechnol. 24, 79–88, 2006.
Popow-Kraupp, T., Aberle, J.H., 2011. Open Microbiol. J. 5, 128–134, 2011.
Romei, M.G., Boxer, S.G., 2019. Annu. Rev. Biophys. 48, 19–44, 2019.

Simoes, E.A.F., 1999. Lancet 354, 847–852, 1999.
Son, J.A., Kim, S.H., Shin, J.H., Jeon, G.W., Sin, J.B., Lee, J.Y., Kim, H.R., Jun, K.R., Lee, J.N., Song, S.A., 2015. Lab. Med. Online 5, 27–32, 2015.
Wang, C., Horby, P.W., Hayden, F.G., Gao, G.F., 2020. Lancet 395, 470–473, 2020.
Zhang, L., Peeples, M.E., Boucher, R.C., Collins, P.L., Pickles, R.J., 2002. J. Virol. 76, 5654–5666, 2002.
Zhu, Q., Patel, N.K., McAuliffe, J.M., Zhu, W., Wachter, L., McCarthy, M.P., Suzich, J.A., 2012. J. Infect. Dis. 205, 635–638, 2012.